Room Temperature Electrochemical Sintering of Zn Microparticles and Its Use in Printable Conducting Inks for Bioresorbable Electronics

Yoon Kyeung Lee, Jeonghyun Kim, Yerim Kim, Jean Won Kwak, Younghee Yoon, and John A. Rogers*

This study describes a conductive ink formulation that exploits electrochemical sintering of Zn microparticles in aqueous solutions at room temperature. This material system has relevance to emerging classes of biologically and environmentally degradable electronic devices. The sintering process involves dissolution of a surface passivation layer of zinc oxide in CH_3COOH/H_2O and subsequent self-exchange of Zn and Zn^{2+} at the Zn/H_2O interface. The chemical specificity associated with the Zn metal and the CH_3COOH/H_2O solution is critically important, as revealed by studies of other material combinations. The resulting electrochemistry establishes the basis for a remarkably simple procedure for printing highly conductive (3×10^5 S m^{-1}) features in degradable materials at ambient conditions over large areas, with key advantages over strategies based on liquid phase (fusion) sintering that requires both oxide-free metal surfaces and high temperature conditions. Demonstrations include printed magnetic loop antennas for near-field communication devices.

Transient electronics represents an emerging class of technology designed to address applications where physical disintegration or chemical dissolution follows a period of stable operation. A particular subset of this field involves biologically environmentally resorbable devices that dissolve in biofluids or ground water to yield benign end products after serving their targeted function.[1–7] Materials and processing techniques are now available for advanced electronics of this type,[3,4,8–12] with supporting device technologies that include primary batteries,[6] sensors,[7] and power scavengers,[2] and offer promise for widespread application in biomedical and consumer products. In such systems, semiconductors such as silicon, conductors such as Mg, and insulators such as silicon nitride serve as high-performance constituent layers formed and processed using deposition and microfabrication techniques adapted from the electronics industry.[3,8,11] Certain components, such as low loss antennas for wireless devices, demand thick conductive traces, ideally formed by methods such as screen or gravure printing. This need establishes the context for the work presented here.

Sintering, an atomic scale diffusion process that can lead to dense, solid materials from powder precursors without bulk melting, represents a commonly used means for joining metal particles to yield conductive traces from printable inks.[13–15] Typically, sintering follows from energy introduced into the system by thermal, optical, or electrical means.[16–18] In certain cases, solid phase sintering can occur spontaneously upon physical contact of two clean surfaces, as with noble metals at low temperatures, sometimes known as cold welding.[19–21] The process can be mediated by certain reducing chemicals as presented in a recent discovery of H_2O_2-induced sintering of nanomaterials.[22] Both types of processes rely on enhanced atomic mobility at free surfaces, but with limited utility in classes of metals that are important for resorbable electronics. Specifically, metals that are attractive for such purposes, such as Mg, Zn, Fe, Mo, and W, include, under ambient conditions, insulating native oxide layers that frustrate sintering due to their high melting temperatures (e.g., ZnO: 1975 °C) and their low diffusivity for transport of the corresponding base metals.[11,23–25] An alternative strategy of using a pulsed laser to selectively evaporate and condensate the inner metal cores of the Zn nanoparticles has recently been suggested as a possible

Y. K. Lee
Department of Chemistry
University of Illinois at Urbana-Champaign
Urbana, IL 61801, USA

Y. K. Lee, Y. Kim, J. W. Kwak, Y. Yoon
Department of Materials Science and Engineering
Frederick Seitz Materials Research Laboratory
University of Illinois at Urbana-Champaign
Urbana, IL 61801, USA

Prof. J. Kim
Department of Electronics Convergence Engineering
Kwangwoon University
Seoul 01897, Republic of Korea

Prof. J. A. Rogers
Center for Bio-Integrated Electronics
Departments of Materials Science and Engineering
Biomedical Engineering, Chemistry, Mechanical Engineering
Electrical Engineering and Computer Science, and Neurological Surgery
Simpson Querrey Institute for Nano/Biotechnology
McCormick School of Engineering, and Feinberg School of Medicine
Northwestern University
Evanston, IL 60208, USA
E-mail: jrogers@northwestern.edu

ADVANCED
SCIENCE NEWS
www.advancedsciencenews.com

ADVANCED
MATERIALS
www.advmat.de

route for construction of thin Zn conducting wires.[26] Electroless deposition, as another alternative for low-temperature fabrication of metal films, has not been reported with bioresorbable metals, possibly due to their strong reducing power, despite its successful demonstration with Cu or Ni.[27–31] As a result, although recent work describes some interesting chemistries suitable for use of some of these metals in inert environments or at elevated temperatures, they have limited applications for the construction of bio/ecoresorbable electronic devices, especially that require thick metal traces over large areas.[4,16,26,32]

The work presented here overcomes this challenge through the use of an electrochemical sintering scheme for aqueous inks that incorporate Zn microparticles. The process relies on exchange of Zn and Zn^{2+}, as distinguished from conventional sintering based on atomic diffusion of the corresponding metal. The chemistry begins with dissolution of the naturally occurring oxide layer by a buffered acidic solution, followed by self-exchange of Zn and Zn^{2+} at the Zn/H_2O interface. The entire process occurs within several minutes at room temperature, resulting a conductivity of $>10^5$ S m^{-1}. This electrical performance exceeds that of previously reported bio/ecoresorbable metal inks.[4,16] Systematic studies of formulations that use other types of acids (HCl and HNO_3) and metals (Fe and Mo) illustrate the chemical specificity of the underlying reactions. Construction of a printed magnetic loop antenna for a simple near-field communication (NFC) device serves to demonstrate an optimized Zn ink processed on a flexible sheet of a bioresorbable polymer (poly lactic-*co*-glycolic acid (PLGA)). The results could have relevance to envisioned uses of bio/ecoresorbable forms of electronics in applications ranging from "green" consumer devices to temporary biomedical implants.

Figure 1a illustrates the mechanism for electrochemical sintering of Zn in aqueous solution. Here, Zn is attractive compared to other biodegradable metals such as Fe, Mo, and W,[11] due to its low activation energy for atomic self-diffusion.[33,34] Key physical and chemical parameters appear in Table S1 (Supporting Information). In ambient conditions, Zn particles include an electrically insulating surface layer, typically tens of nanometers in thickness, formed by spontaneous oxidation.[25,35] Specifically, upon exposure to humid air, oxidation leads to the formation of ZnO and $Zn(OH)_2$ at the surface, which slowly convert to zinc hydroxycarbonates $Zn_4CO_3(OH) \cdot 6H_2O$ and $Zn_5(CO_3)_2 \cdot (OH)_6$, respectively.[25,34] The composition, crystallinity, and thickness of this layer depend on the exposure time and the characteristics of the surrounding environment. An aqueous solution of acetic acid ($H_2O{:}CH_3COOH = 10{:}1$ by volume, pH 2.3) can dissolve this native passivation layer, largely independent of its details, thereby exposing the bare metal surface. Under acidic and static hydrodynamic conditions, this dissolution also promotes self-exchange between Zn and Zn^{2+} at the Zn/H_2O interfaces between the particles. The result "welds" the particles together into a percolating, conductive network. As the solvent evaporates, the acetate anion (CH_3COO^- (ac), $pK_a = 4.8$) produced from the corrosion reaction of Zn and CH_3COOH buffers the solution until the ink is fully dry, at which point the welded compact solid becomes covered with a new passivation layer ($Zn(ac)_2$).

The details of the electrochemistry appear in Figure 1b–d. Immersion of Zn into an aqueous solution initiates electrochemical reactions at the Zn/H_2O interface. Destabilization of the surface oxide layer in acids can be described by the potential–pH equilibrium diagram (Pourbaix diagram) of the Zn/H_2O system, as shown in Figure 1b.[36] The solid lines represent Nernst scaling for Zn^{2+}/Zn (purple, 10×10^{-3} M Zn^{2+}), $Zn(OH)_2/Zn$ (black), H^+/H_2 (orange) for reactions that are involved at the Zn surface (Equations (1)–(3)).

$$Zn^{2+} + 2e \rightleftharpoons Zn, \quad E(V_{SHE}) = -0.76 + 0.0295\log\left[Zn^{2+}\right] \tag{1}$$

$$\begin{aligned}Zn(OH)_2 + 2H^+ + 2e &\rightleftharpoons Zn + 2H_2O, \\ E(V_{SHE}) &= -0.44 - 0.0591\,pH\end{aligned} \tag{2}$$

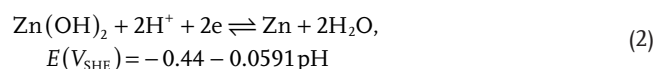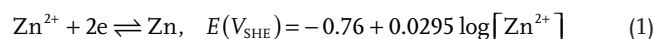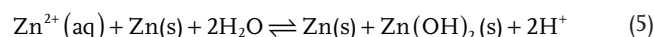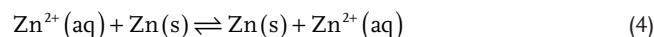$$2H^+ + 2e \rightleftharpoons H_2, \quad E(V_{SHE}) = 0.00 - 0.0591\,pH \tag{3}$$
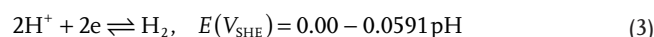
Figure 1c,d outlines the electrochemical behavior of Zn in CH_3COOH/H_2O real systems. The open circuit voltage (OCV) of Zn powders (<10 μm) fixed on Cu tape measured in deionized (DI) water (30 mL) and in the same solution after adding CH_3COOH reveal the major electrochemical reactions. Zn foil electrodes (5 mm × 5 mm × 250 μm), without the Cu tape, exhibit similar OCV behaviors, indicating that the electrochemical reactions associated with the Zn surface are similar for powders and bulk samples.) Figure 1c shows that the rest potential of the Zn electrode in DI water lies near the reduction potentials of H^+ (Equation (3)). The OCV is slightly lower than the reduction potential of H^+ due partially to oxidation of Zn in near-neutral water. As a result, Zn metal deposition is unlikely to occur, as predicted from the Pourbaix diagram.

Addition of CH_3COOH (1 mL), however, reduces the OCV dramatically, to levels where Zn deposition can occur. Specifically, the OCV measured near the reduction potential of Zn^{2+}/Zn reflects that CH_3COOH shifts the equilibrium toward the Zn^{2+}/Zn redox reaction. Self-exchange, concurrent with dissolution of the metal and deposition of the metal from aqueous Zn^{2+}, results in the relocation of Zn metal atoms. Another possible self-exchange mechanism is through mediation associated with the $Zn(OH)_2/Zn$ half reaction, which can be significant at high local pH on the Zn surface (Equations (4) and (5)).

$$Zn^{2+}(aq) + Zn(s) \rightleftharpoons Zn(s) + Zn^{2+}(aq) \tag{4}$$

$$Zn^{2+}(aq) + Zn(s) + 2H_2O \rightleftharpoons Zn(s) + Zn(OH)_2(s) + 2H^+ \tag{5}$$

Although OCVs provide information on the electrochemical reactions, dynamic information such as the rate of self-exchange between Zn^{2+} and Zn must obtained through measurements of currents induced by polarizing the Zn away from the OCV. Figure 1d shows polarization curves of Zn in $Zn(ac)_2$ solutions, in which the voltage of the Zn electrode varies from +250 to −250 mV from its OCV, without agitation. Shifts of the polarization curves to larger currents with increasing Zn^{2+} support the occurrence of self-exchange reactions on the Zn surface. Similar polarization curves obtained with K(ac), a salt with the same anion as $Zn(ac)_2$ but with a cation that cannot be reduced at these voltage levels, at the same pH (green, Figure 1d) confirm that the cathodic current
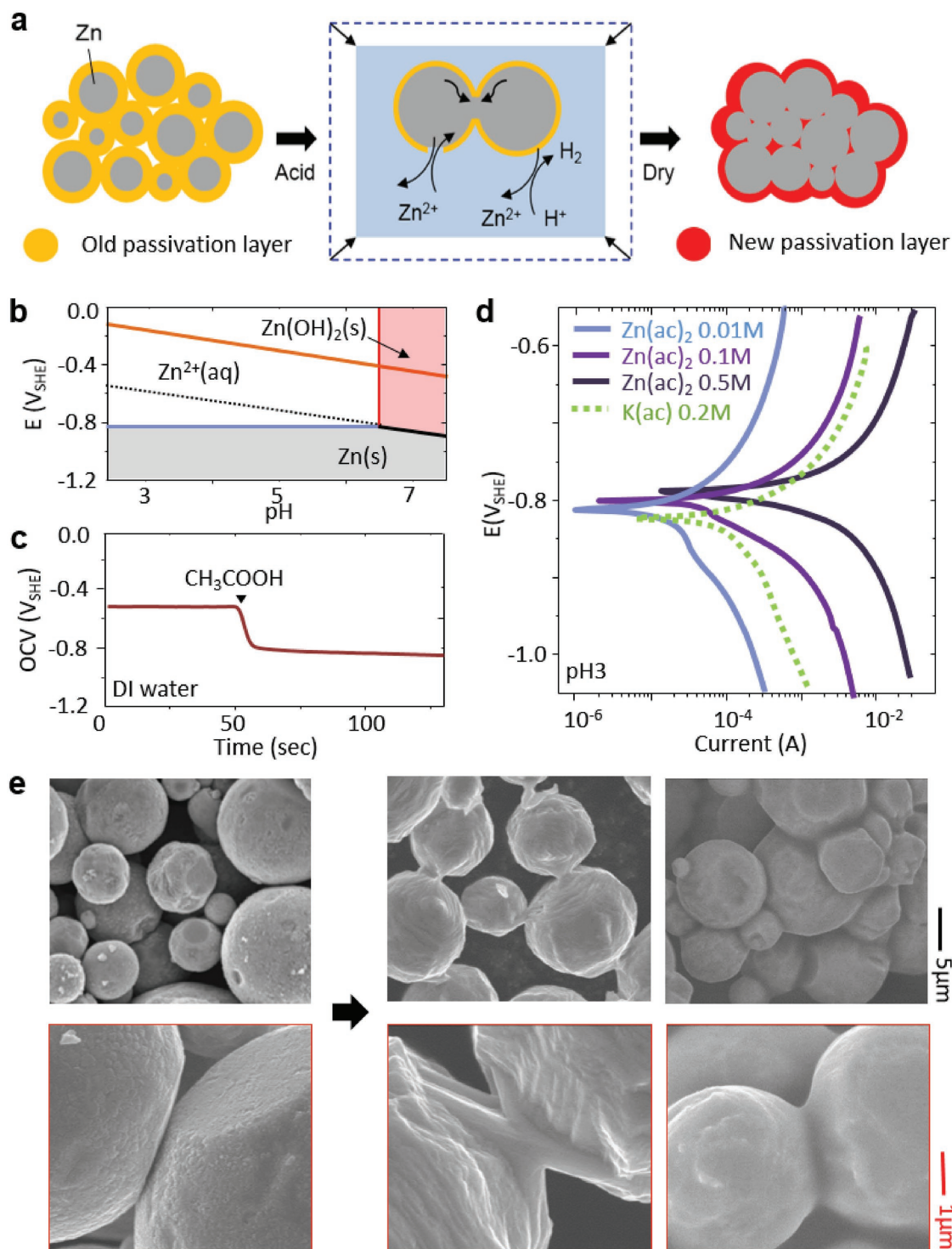
Figure 1. Electrochemical sintering of Zn microparticles in CH_3COOH/H_2O. a) Proposed mechanism for electrochemical Zn sintering. b) Pourbaix diagram of Zn in aqueous solution. c) Change in OCV after addition of CH_3COOH. d) Polarization curves with various concentrations of $Zn(ac)_2$ at pH 3. e) Morphology of Zn before/after exposure to CH_3COOH/H_2O.

at OCV originates from reduction of Zn^{2+}. Here, as expected, scans of voltage negative relative to OCV show reduced cathodic current compared to $Zn(ac)_2$ due to the reduced concentration of Zn^{2+} on the Zn surface.

The deposition of Zn from Zn^{2+} can sinter adjacent particles of Zn. Figure 1e illustrates the morphological changes of Zn particles that occur after immersion in H_2O/CH_3COOH (10:1 by volume, pH 2.3) for less than a minute followed by

**ADVANCED
SCIENCE NEWS**

www.advancedsciencenews.com
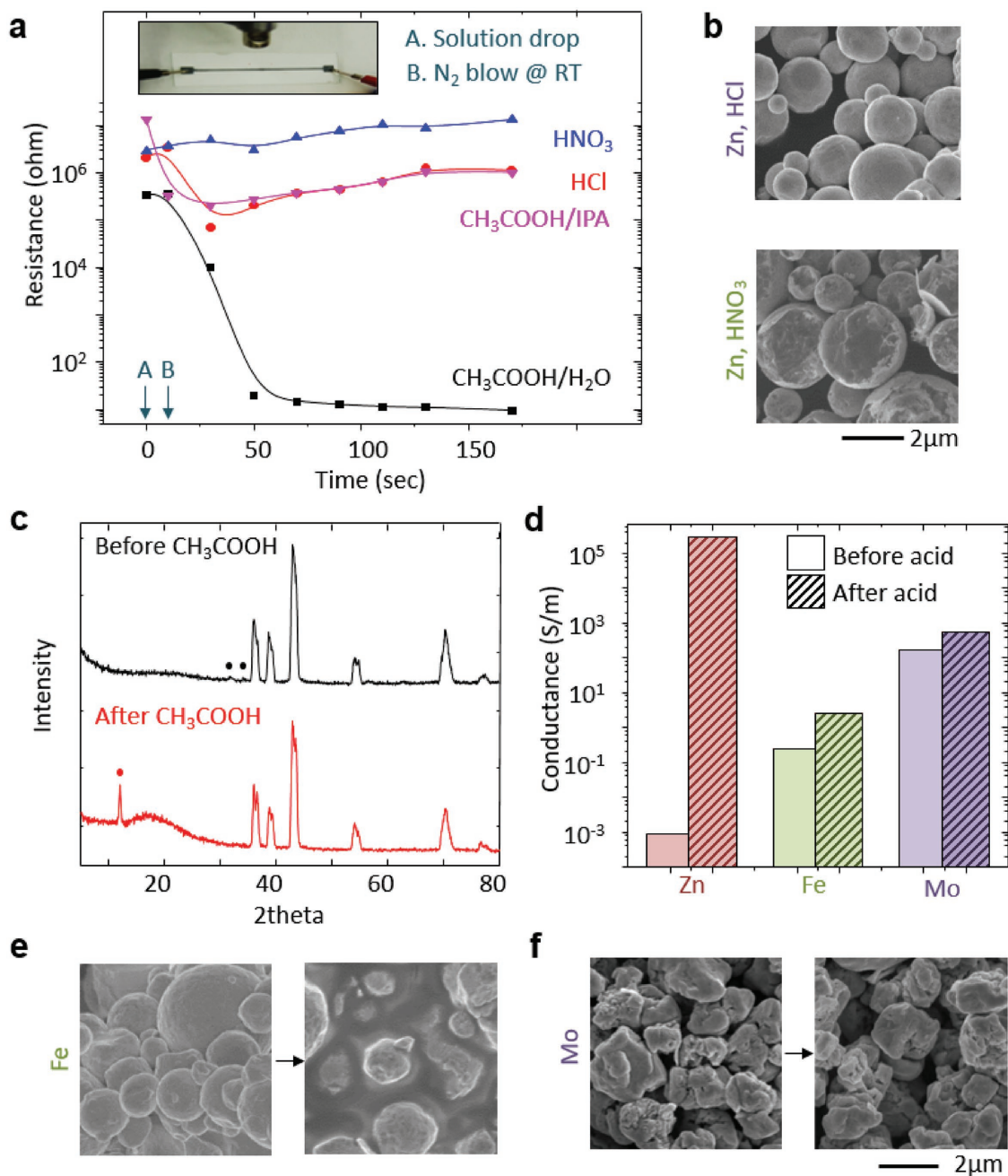
**ADVANCED
MATERIALS**

www.advmat.de

Figure 2. Comparative study with other acids and metals. a) Change in resistance after treatment with CH_3COOH, HCl, and HNO_3 (pH 2.3). b) Morphology of Zn after treatment with HCl and HNO_3. c) X-ray diffraction patterns of printed deposits of Zn. d) Conductivities of Zn, Fe, and Mo inks before and after treatment with CH_3COOH/H_2O. e,f) Morphology of e) Fe and f) Mo before/after treatment with CH_3COOH/H_2O.

drying with a stream of nitrogen at room temperature and ambient conditions. The initial state corresponds to a collection of particles dispersed in DI water and drop cast onto a piece of carbon tape. The images in the second column show the formation of necks at points of near contact between the particles, corresponding to regions of high local concentration of Zn. The images in the right column highlight the transformation into a solid compact covered with a thick passivation layer when the interparticle distances are sufficiently short. This sintering process yields macroscopic pores (≈50 μm)

due to shrinkage of the interparticle distance (Figure S2, Supporting Information). Comparison to results from inks with other acids and metals provides additional insights, as explained subsequently.

Figure 2a shows the change in electrical conductivity measured in patterns printed through a stencil mask using an ink formulation of Zn particles mixed with polyvinylpyrrolidone (PVP) as a binder in isopropyl alcohol (IPA) (Zn:PVP:IPA = 30:1:10 by weight) to facilitate printing. PVP is attractive due to its solubility in IPA and water, its nontoxicity, and widespread

use in stabilizing particle suspensions owing to possible coordination of N and O atoms present in PVP to the metals.[13–15] The porosity of the printed metal lines is ≈30%, as estimated on the basis of densities of the Zn particles (7.133 g cm^{-3}) and the PVP (1.2 g cm^{-3}). The initial resistances of patterns that consist of 1-mm-wide, 6-cm-long, and ≈50-µm-thick lines on glass slides reduce from >10 MOhm to <10 Ohm due to treatment with CH_3COOH/H_2O (drop casting of <100 µL, 1:10 by volume). The effect of exposure time is minimal since the removal of the surface oxide layer and the particle welding are completed in a short time. Other acidic solutions (HCl and HNO_3 in H_2O) with pH values between 1.5 and 4 show much smaller improvement in conductivity, as shown for pH 2.3 in Figure 2a. Such cases involve an initial decrease in the resistance, mainly due to removal of Zn oxides, but the resistance increases again after drying due to the reformation of these oxides. Figure 2b shows images that indicate that the representative surface morphologies of the Zn particles are either unchanged (for treatment with HCl) or undergo severe corrosion (HNO_3). Additional experiments indicate that changing the solvent from H_2O to IPA diminishes the ability of CH_3COOH to improve the resistance, possibly due to a low rate of self-exchange of Zn^{2+}/Zn and/or a low solubility of $Zn(ac)_2$ in IPA. Metal traces (≈50 µm) printed onto flexible substrates (Kapton (thickness 75 µm) and PLGA (≈50 µm), both with a ≈5 µm top layer of PLGA) maintain their electrical conductivity upon bending to radii of curvature as small as 5 mm (maximum bending strain: ≈1%) without delamination or cracking (Figures S7 and S10, Supporting Information). X-ray diffraction patterns (Figure 2c) of zinc before/after CH_3COOH treatment suggest no significant change in crystallinity. Small peaks associated with ZnO (black dots) in the sample before treatment arise from the passivation layer. The sample after treatment shows a large peak that corresponds to $Zn(ac)_2$ (red dot)[37] from Zn^{2+} and deprotonated CH_3COO^- due to corrosion reactions between Zn metal and CH_3COOH, which indicates that the local concentration of CH_3COO^- on the Zn surface can be high with exposure to small volumes of CH_3COOH/H_2O during the acid treatment and drying. Prolonged exposure to high concentration of CH_3COO^- in water ($Zn(ac)\cdot H_2O:H_2O:Zn:PVP = 10:30:4:1.5$ (w/v%), 10 min) with agitation results in an increase in the (001) peak of Zn metal, consistent with possible Zn diffusion induced by chemically specific interactions between Zn^{2+} and CH_3COO^- (Figure S5, Supporting Information).

Figure 2d summarizes the electrical properties of inks based on Zn compared to those formed with other reactive metals, Fe and Mo. The test structures involve line patterns printed with these three inks (Zn, Fe, and Mo) on Au contact pads near the ends (Figure S6c, Supporting Information). The conductivity corresponds to the slope of the measured resistance as a function of length, using the cross-sectional area of the lines. The relative values of the initial conductivities are Zn < Fe < Mo, consistent with the relative reactivities of these metals, as compared by their standard reduction potentials in Table S1 (Supporting Information), ($E^o(V_{SHE}) = -0.76$ (Zn^{2+}/Zn), -0.44 (Fe^{2+}/Fe), -0.2 V (Mo^{3+}/Mo)). Reactive metals tend to form thick native oxides, thereby leading to reduced conductivity. After treatment with diluted CH_3COOH, the conductivity for all three cases increases as a result of dissolution of their native

oxide layers. Zn shows an increase of eight orders of magnitude, from 10^{-3} to 10^5 S m^{-1}, with good stability (degradation rate of <10^4 S m^{-1} per day in ambient air) (Figure S6g, Supporting Information). When stored in a desiccator with anhydrous calcium sulfate, the conductivity remains unchanged over a period of 3 weeks. This sintering scheme is also applicable to nanosized particles (<200 nm), where an increase in the conductivity by five orders of magnitude from 1.1×10^{-3} to 6.1×10^2 S m^{-1} follows from processing under ambient conditions (Figure S4, Supporting Information). Fe, whose reduction potential is between Zn and Mo, shows a modest improvement, i.e., 10^{-1}–10 S m^{-1}. The effect is more limited in Mo. Figure 2e,f shows the surfaces of Fe and Mo. Fe is covered by corrosion products, possibly due to preference of H$^+$ reduction instead of Fe^{2+} reduction. Table S1 (Supporting Information) summarizes reported hydrogen exchange currents (H^+/H_2), which are larger on Fe and Mo compared to Zn.[38–43] Mo does not show any morphological change.

Figure 3 demonstrates screen printing of the Zn ink (800 µm line width) to yield a radio frequency (RF) antenna for a simple NFC device. NFC technology is increasingly appearing in wireless tags and sensors for banking, biomedicine, and transportation due its ability to provide a low cost electronic interface to external readers such as a smartphones.[44–46] More broadly, NFC platforms are projected to have a prominent role in internet-of-things devices, where proliferation could occur at a scale with potential adverse environmental consequences. In this context, a bioresorbable conductive ink could eliminate waste streams associated with certain elements, such as antennas and associated interconnects. Figure 3a describes the fabrication. The first step is to prepare a biodegradable film of PLGA by drop casting a solution of PLGA (20 w/v% in ethyl acetate) on a glass substrate. The screen printing process is shown in Figure 3a,ii (Zn:PVP:IPA = 3:0.1:1 by weight). Here, PVP increases the viscosity to facilitate printing. The white printed lines correspond to the Zn ink in its high resistance state, which becomes conductive after treatment with a solution of water and CH_3COOH (water:CH_3COOH:PVP = 10:0.5:2 w/v%) (Figure 3a, iii). Migration of PLGA into the pores between the metal particles during the heating steps results in excellent adhesion (Figures S9 and S10, Supporting Information). The patterns maintain their shape during the wet sintering process owing to the low solubility of PLGA in water. The degradation of PLGA occurs on time scales that are much longer than those required for the wet sintering process (≈10 min including the drying process).[47] Interconnecting the two terminals of the antenna, mounting an NFC chip and a light-emitting diode (LED), and drop-casting PLGA (20 w/v% in ethyl acetate, ≈100 µm) on top as an encapsulation layer complete the device (Figure 3a, vi). The PLGA overcoat permeates through the pores, thereby protecting the particles from direct contact to the air and water without affecting the electrical connection between the particles (Figure S8, Supporting Information). Figure 3b shows a device. Figure 3c–f corresponds to frames from Movie S1 (Supporting Information) that highlights the functionality. In Figure 3c, an LED connected to the antenna demonstrates wireless power harvesting from an external RF source. Figure 3d shows digital readings of changes in temperature wirelessly captured using a smartphone during heating with a heat gun. Other functions,
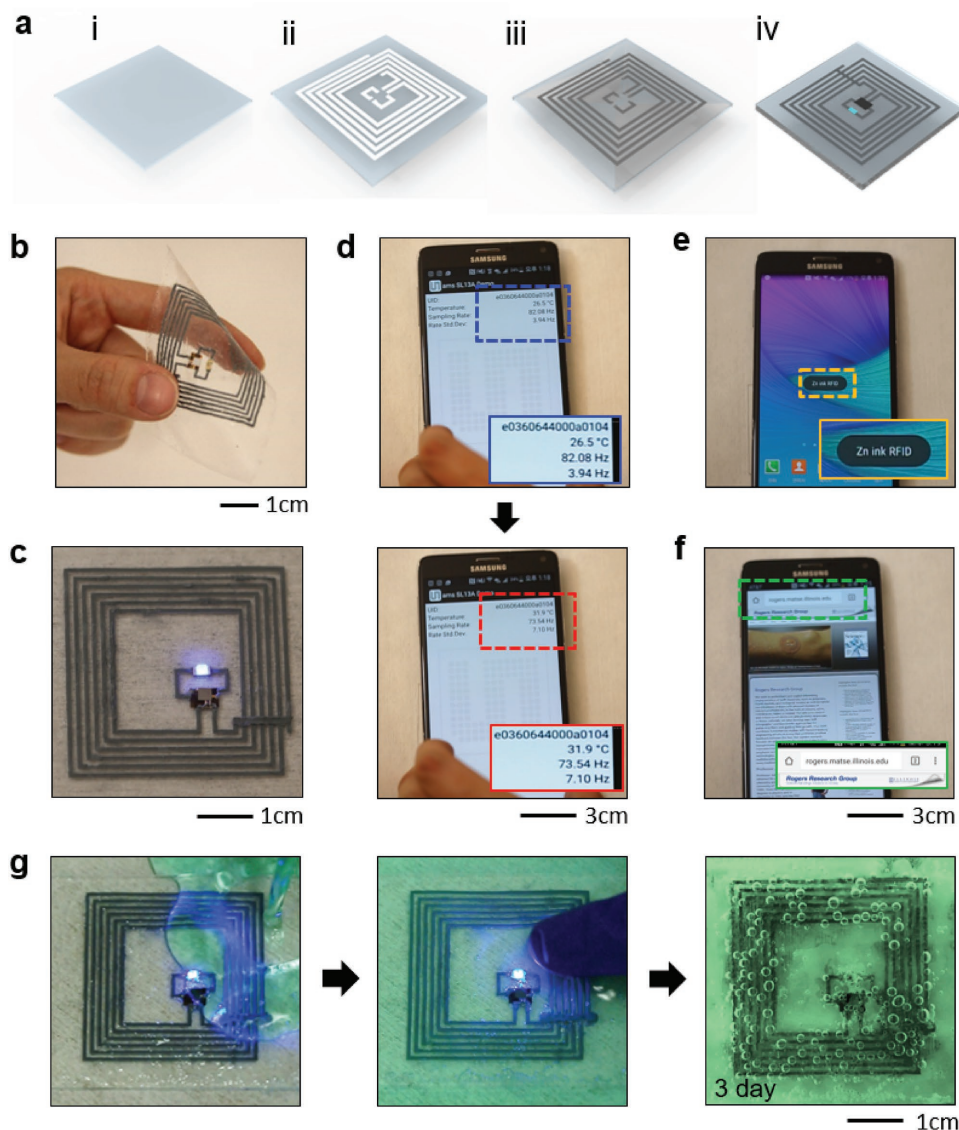
Figure 3. Demonstration of NFC devices with Zn ink. a) Schematic illustration of the fabrication process. b) Images of an NFC device. c–f) Series of images that demonstrate wireless communication with a smartphone, as captured from Movie S1 (Supporting Information). c) LED operated by wireless power transfer through the RF antenna; d) wireless readout of temperature with a smartphone; e) identification and f) automatic webpage launch achieved through wireless communication. g) Water compatibility of the device and degradation behavior with PLGA encapsulation.

such as automatic launching of a website and identification, are featured in Figure 3e,f.

Figure 3g illustrates the process of degradation by immersion in water. The device remains functional for several hours (without agitation) with a 100 µm PLGA coating. Degradation of the Zn leads to visible bubbles of hydrogen, as shown in Figure 3g, after several days. PLGA undergoes slow degradation in aqueous solution through the breakage of its ester bonds.[47]

This paper describes a process of acid-induced, rapid (few minutes) sintering of Zn metal particles under ambient conditions, without heating or mechanical loading. Unlike conventional sintering schemes that rely on atomic diffusion, the mechanism reported here involves dissolution of native oxides followed by electrochemical self-exchange of Zn and

Zn^{2+}. Systematic studies with various types of acids and metals reveal important factors in this process. Wireless devices with interconnects and antennas of conductive traces formed by printing of optimized Zn inks show excellent performance. As a bioresorbable printable conductor, the chemistry reported here offers broad potential applications in environmentally sustainable electronic devices and advanced, temporary biomedical implants.

Experimental Section

Fabrication and Printing of the Zn Ink: A solution of Zn (<10 µm, Sigma Aldrich) and PVP (molecular weight 360 000, Sigma Aldrich) in IPA involved mixing constituents at a ratio of Zn:PVP:IPA = 3:0.1:1 by

**ADVANCED
SCIENCE NEWS**

www.advancedsciencenews.com

**ADVANCED
MATERIALS**

www.advmat.de

weight. Other metal inks (e.g., Mo, Fe; <10 µm, Sigma Aldrich) used the same ratio. Screen printing involved a stencil mask placed against a target substrate of either glass or PLGA (Sigma Aldrich). Drying with an N_2 gun (Figures 1g and 2a) or by heating at 70 °C in an oven ensured complete solvent evaporation (for other experiments). All experiments were conducted in air under ambient conditions.

Acid Treatment and Conductivity Measurements: A mixture of CH_3COOH and distilled water (1:10 by volume) dropcast on the dried metal patterns eliminated the oxide layer and initiated the sintering process (Figure 1a). For other experiments, a formulation with PVP (water:CH_3COOH:PVP = 10:0.5:2 w/v%) helped to maintain the physical integrity of the printed features during the acid treatment. Reported conductivities corresponded to measurements either directly on the printed pattern (Figure 2a) or through Au contact pads formed by electron beam evaporation (Figure 2d).

Measurements of Polarization Curves: Solutions of $Zn(CH_3COOH)\cdot 2H_2O$ and $K(CH_3COOH)$ with the desired molarity were titrated with HCl to the desired pH. A saturated Ag/AgCl electrode (BASi, USA) served as a reference electrode. Working electrodes involved bulk metal foils or metal powder by fixed on Cu tape. These two types of electrodes showed the same response upon stirring, acid addition, and polarization. To obtain the polarization curves, bulk metal electrodes (Zn, Fe, or Mo; 5 mm × 5 mm × 250 µm foil, Sigma Aldrich) were scanned from +250 to −250 mV from stabilized open-circuit potentials in different solutions to obtain the present polarization curves by using a GAMRY Reference 6000 potentiostat/galvanostat (GAMRY, USA).

Fabrication of the NFC Device: The process began with printing the coil pattern (50–100 µm) with an ink formulation of Zn:PVP:IPA = 3:0.1:1 by weight. A solution of PVP, water, and CH_3COOH (water:CH_3COOH:PVP = 10:0.5:2 w/v%) coated on top of the printed patterns initiated the sintering process for the Zn particles. After acid activation, drop casting of PLGA dissolved in ethyl acetate formed an overcoat except for the ends of the features. Mounting the NFC chip (SL13A, AMS AG) and LED onto the coil with some additional Zn ink, followed by casting of CH_3COOH:H_2O = 10:1 (by volume), yielded an electrically connected system. Electromagnetic characterization used an impedance analyzer (4291A RF impedance/material analyzer, Hewlett Packard) with a wound coil. Figure S11 (Supporting Information) presents the phase response of the device.

Supporting Information

Supporting Information is available from the Wiley Online Library or from the author.

Acknowledgements

Conflict of Interest

The authors declare no conflict of interest.

Keywords

[1] C. H. Lee, S.-K. Kang, G. A. Salvatore, Y. Ma, B. H. Kim, Y. Jiang, J. S. Kim, L. Yan, D. S. Wie, A. Banks, S. J. Oh, X. Feng, Y. Huang, G. Troester, J. A. Rogers, *Adv. Funct. Mater.* **2015**, *25*, 5077.

[2] S.-W. Hwang, X. Huang, J.-H. Seo, J.-K. Song, S. Kim, S. Hage-Ali, H.-J. Chung, H. Tao, F. G. Omenetto, Z. Ma, J. A. Rogers, *Adv. Mater.* **2013**, *25*, 3526.

[3] S.-W. Hwang, H. Tao, D.-H. Kim, H. Cheng, J.-K. Song, E. Rill, M. A. Brenckle, B. Panilaitis, S. M. Won, Y.-S. Kim, Y. M. Song, K. J. Yu, A. Ameen, R. Li, Y. Su, M. Yang, D. L. Kaplan, M. R. Zakin, M. J. Slepian, Y. Huang, F. G. Omenetto, J. A. Rogers, *Science* **2012**, *337*, 1640.

[4] X. Huang, Y. Liu, S.-W. Hwang, S.-K. Kang, D. Patnaik, J. F. Cortes, J. A. Rogers, *Adv. Mater.* **2014**, *26*, 7371.

[5] S.-W. Hwang, G. Park, H. Cheng, J.-K. Song, S.-K. Kang, L. Yin, J.-H. Kim, F. G. Omenetto, Y. Huang, K.-M. Lee, J. A. Rogers, *Adv. Mater.* **2014**, *26*, 1992.

[6] L. Yin, X. Huang, H. Xu, Y. Zhang, J. Lam, J. Cheng, J. A. Rogers, *Adv. Mater.* **2014**, *26*, 3879.

[7] S.-K. Kang, R. K. J. Murphy, S.-W. Hwang, S. M. Lee, D. V. Harburg, N. A. Krueger, J. Shin, P. Gamble, H. Cheng, S. Yu, Z. Liu, J. G. McCall, M. Stephen, H. Ying, J. Kim, G. Park, R. C. Webb, C. H. Lee, S. Chung, D. S. Wie, A. D. Gujar, B. Vemulapalli, A. H. Kim, K.-M. Lee, J. Cheng, Y. Huang, S. H. Lee, P. V. Braun, W. Z. Ray, J. A. Rogers, *Nature* **2016**, *530*, 71.

[8] S.-K. Kang, S.-W. Hwang, H. Cheng, S. Yu, B. H. Kim, J.-H. Kim, Y. Huang, J. A. Rogers, *Adv. Funct. Mater.* **2014**, *24*, 4427.

[9] S.-W. Hwang, J.-K. Song, X. Huang, H. Cheng, S.-K. Kang, B. H. Kim, J.-H. Kim, S. Yu, Y. Huang, J. A. Rogers, *Adv. Mater.* **2014**, *26*, 3905.

[10] S.-W. Hwang, G. Park, C. Edwards, E. A. Corbin, S.-K. Kang, H. Cheng, J.-K. Song, J.-H. Kim, S. Yu, J. Ng, J. E. Lee, J. Kim, C. Yee, B. Bhaduri, Y. Su, F. G. Omennetto, Y. Huang, R. Bashir, L. Goddard, G. Popescu, K.-M. Lee, J. A. Rogers, *ACS Nano* **2014**, *8*, 5843.

[11] L. Yin, S. Mao, R. T. Haasch, Y. Liu, X. Xie, S.-W. Hwang, H. Jain, S.-K. Kang, R. Li, Y. Huang, J. A. Rogers, *Adv. Funct. Mater.* **2014**, *24*, 645.

[12] S.-W. Hwang, D.-H. Kim, H. Tao, T.-i. Kim, S. Kim, K. J. Yu, B. Panilaitis, J.-W. Jeong, J.-K. Song, F. G. Omenetto, J. A. Rogers, *Adv. Funct. Mater.* **2013**, *23*, 4087.

[13] D. Kim, J. Moon, *Electrochem. Solid-State Lett.* **2005**, *8*, J30.

[14] B. K. Park, D. Kim, S. Jeong, J. Moon, J. S. Kim, *Thin Solid Films* **2007**, *515*, 7706.

[15] A. Kamyshny, J. Steinke, S. Magdassi, *Open Appl. Phys. J.* **2011**, *4*, 19.

[16] B. Mahajan, X. Yu, W. Shou, H. Pan, X. Huang, *Small* **2017**, *13*, 1700065.

[17] N. R. Bieri, J. Chung, D. Poulikakos, C. P. Grigoropoulos, *Superlattices Microstruct.* **2004**, *35*, 437.

[18] M. Allen, M. Aronniemi, T. Mattila, A. Alastalo, K. Ojanpera, *Nanotechnology* **2008**, *19*, 175201.

[19] S. Magdassi, M. Grouchko, O. Berezin, A. Kamyshny, *ACS Nano* **2010**, *4*, 1943.

[20] Y. Lu, J. Y. Huang, C. Wang, S. Sun, J. Lou, *Nat. Nanotechnol.* **2010**, *5*, 218.

[21] G. S. Ferguson, M. K. Chaudhury, G. B. Sigal, G. M. Whitesides, *Science* **1991**, *253*, 776.

[22] S.-S. Yoon, D.-Y. Khang, *Nano Lett.* **2016**, *16*, 3550.

[23] Z. A. Munir, *J. Mater. Sci.* **1979**, *14*, 2733.

[24] L. Gunawan, G. P. Johari, *J. Phys. Chem. C* **2008**, *112*, 20159.

[25] Y. Chen, P. Schneider, A. Erbe, *Phys. Status Solidi* **2012**, *209*, 846.

[26] W. Shou, B. K. Mahajan, B. Ludwig, X. Yu, J. Staggs, X. Huang, H. Pan, *Adv. Mater.* **2017**, *29*, 1700172.

[27] Y. Yu, X. Xiao, Y. Zhang, K. Li, C. Yan, X. Wei, L. Chen, H. Zhen, H. Zhou, S. Zhang, Z. Zheng, *Adv. Mater.* **2016**, *28*, 4926.

[28] K. Li, H. Zhen, L. Niu, X. Fang, Y. Zhang, R. Guo, Y. Yu, F. Yan, H. Li, Z. Zheng, *Adv. Mater.* **2014**, *26*, 7271.

[29] Y. Yu, C. Yan, Z. Zheng, *Adv. Mater.* **2014**, *26*, 5508.

[30] R. Guo, Y. Yu, Z. Xie, X. Liu, X. Zhou, Y. Gao, Z. Liu, F. Zhou, Y. Yang, Z. Zheng, *Adv. Mater.* **2013**, *25*, 3343.

[31] Z. Zhao, C. Yan, Z. Liu, X. Fu, L.-M. Peng, Y. Hu, Z. Zheng, *Adv. Mater.* **2016**, *28*, 10267.

[32] B. K. Mahajan, X. Yu, W. Shou, H. Pan, X. Huang, *Small* **2017**, *13*, 1700065.

[33] G. Neumann, C. Tuijn, *Self-Diffusion and Impurity Diffusion in Pure Metals: Handbook of Experimental Data*, Pergamon, Oxford, United Kingdom **2009**.

[34] X. G. Zhang, *Corrosion and Electrochemistry of Zinc*, Springer, New York City, USA **1996**.

[35] J. Zuo, A. Erbe, *Phys. Chem. Chem. Phys.* **2010**, *12*, 11467.

[36] M. Pourbaix, *Atlas of Electrochemical Equilibria in Aqueous Solutions*, National Association of Corrosion Engineers, Texas, USA **1974**.

[37] M. M. Demir, R. Munoz-Espi, I. lieberwirth, G. Wegner, *J. Mater. Chem.* **2006**, *16*, 2940.

[38] J. R. Davis, *Corrosion: Understanding the Basics*, ASM International, Ohio, USA **2000**.

[39] L. Sziraki, E. Szocs, Z. Pilbath, K. Papp, E. Kalman, *Electrochim. Acta* **2001**, *46*, 3743.

[40] B. N. Popov, *Corrosion Engineering: Principles and Solved Problems*, Elsevier, Amsterdam, Netherlands **2015**.

[41] F. C. Porter, *Zinc Handbook: Properties, Processing, and Use In Design*, CRC Press, Florida, USA **1991**.

[42] S. Trasatti, *J. Electroanal. Chem.* **1972**, *39*, 163.

[43] Y. Yan, B. Y. Xia, B. Zhao, X. Wang, *J. Mater. Chem. A* **2016**, *4*, 17587.

[44] J. Kim, A. Banks, Z. Xie, S. Y. Heo, P. Gutruf, J. W. Lee, S. Xu, K.-I. Jang, F. Liu, G. Brown, J. Choi, J. H. Kim, X. Feng, Y. Huang, U. Paik, J. A. Rogers, *Adv. Funct. Mater.* **2015**, *25*, 4761.

[45] J. Kim, A. Banks, H. Cheng, Z. Xie, S. Xu, K.-I. Jang, J. W. Lee, Z. Liu, P. Gutruf, X. Huang, P. Wei, F. Liu, K. Li, M. Dalal, R. Ghaffari, X. Feng, Y. Huang, S. Gupta, U. Paik, J. A. Rogers, *Small* **2015**, *11*, 906.

[46] J. Kim, P. Gutruf, A. M. Chiarelli, S. Y. Heo, K. Cho, Z. Xie, A. Banks, S. Han, K.-I. Jang, J. W. Lee, K.-T. Lee, X. Feng, Y. Huang, M. Fabiani, G. Gratton, U. Paik, *Adv. Funct. Mater.* **2017**, *27*, 1604373.

[47] R. A. Jain, *Biomaterials* **2000**, *21*, 2475.